Numerical and Experimental Studies of Simple Geometries in Slamming

Adrian Constantinescu
ANAST, University of Liege
Liege, Belgium

Aboulghit El Malki Alaoui
LBMS - EA 4325 - ENSIETA
Brest, France

Alain Nême
LBMS - EA 4325 - ENSIETA
Brest, France

Philippe Rigo
ANAST, University of Liege
Liege, Belgium

ABSTRACT

The paper presents a numerical and experimental study of slamming phenomena experienced by rapid ships during the impact of its bow on the water surface. The research work covers the finite element modeling of the impact between a rigid body and a free water surface using three numerical approaches based on the finite element code ABAQUS, as well as experimental slamming tests for validation.

KEY WORDS: Slamming; Shock machine; Fluid-structure interaction; ABAQUS/Explicit; Coupled Eulerian-Lagrangian (CEL).

INTRODUCTION

Initially studied for seaplane floats (Von Karman, 1929; Wagner, 1932), the slamming phenomena quickly began important in the naval field. This dynamic, random and non-linear impact induces local and global harmful effects. Concerning the global responses, the whole ship is brutally subjected to additional bending moment and shearing force, introducing general vibrations of the beam hull ship. The local response describes more especially the local damages due to repeated impacts on the exterior hull. Theses responses affect also the crew and passengers comfort and the integrity of embarked equipments. In these conditions, it is important to predict exactly the applied forces for a correct and optimal design.

According to Bertram (2002), the wave impact caused by the slamming can be roughly classified into four types: bottom, 'bow-flare', breaking wave and wet-deck. This paper treats only the bottom slamming, i.e. impact between the inferior hull structure and the free water surface. Even if the slamming is a fully three-dimensional phenomenon, we limit our study to simple rigid geometries (2D and pseudo-3D) and 2D flows, as a first step to develop numerical methods for deformable and 3D cases. Slamming forces depend on the deadrise angle between body and free water surface. With air trapping the mechanism of impact becomes more complex. The effects generated by the presence of air cannot be neglected for deadrise angles lower than 4° (Langrand, 2001). Our study is then limited to deadrise angles between 4° and 45° according to Wagner theory.

ABAQUS/STANDARD APPROACH

Mathematical formulation

We consider the impact problem of a body on a water surface, according to the Fig. 1. The fluid problem is formulated within potential flow theory for an ideal fluid (incompressible, inviscid, irrotational), initially at rest. We assume small disturbances for the fluid and the solid domain, and we neglect the gravity. The structure has no forward speed and the current is zero. The flow is analyzed using eulerian variables and must fulfill the conservation of mass and the momentum equation. The velocity vector anywhere in the fluid domain is obtained as $V_f = \mathbf{grad}\,\Phi$ and the velocity potential $\Phi(x,y,z,t)$ must satisfy the continuity, sliding, free surface condition and decay conditions respectively, Eqs. 1~4.

$\Delta\Phi = 0$	in the fluid domain Ω_f	(1)
$\mathbf{grad}\,\Phi \cdot \mathbf{n} = V_S \cdot \mathbf{n}$	on the wetted surface Γ_B	(2)
$\Phi = 0$	on the free surface Γ_L	(3)
$\mathbf{grad}\,\Phi = 0$	far from the body Γ_∞	(4)

Keeping non-linear limit conditions, the fluid problem is very complex. To simplify the fluid formulation, previous limit conditions will be projected on the initial water surface (z = 0). The free surface is a

material surface. Its elevation *h*, relative to its initial position, allows us to write a kinematic boundary condition for the free surface, Eq. 5, keeping liner terms in the wave amplitude. The non-stationary version of the Bernoulli equation establishes the formula for the hydrodynamic pressure, Eq. 6. In this equation, the second term represents the steady state dynamic pressure. The values of the pressure are non-null only on the surface in contact with the body.

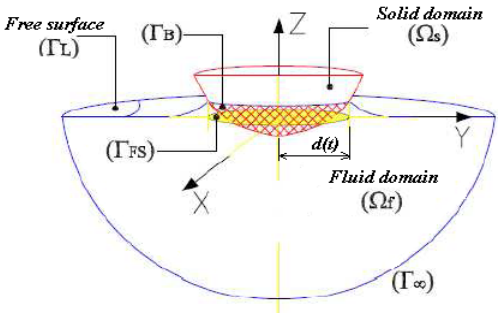

Fig. 1 – Geometric definition

$$\frac{\partial \Phi}{\partial z} = \frac{\partial h}{\partial t} \quad \text{on the free surface, where } h = \int_0^t \left.\frac{\partial \Phi}{\partial z}\right|_{(x,y,0,\tau)} d\tau \tag{5}$$

$$p = -\rho_f \frac{\partial \Phi}{\partial t} - \frac{1}{2}\rho_f \left(\mathbf{grad}\Phi\right)^2 \tag{6}$$

The extent of the wet surface, denoted $d(t)$ in Fig. 1, represents the intersection between the free surface rising and the position of the solid body. The integral in time of the normal derivative of the velocity potential expresses the free surface elevation. Thus, we can solve the problem of the displacement potential $\Psi = \Psi(x, y, z, t)$ such that:

$$\Psi = \int_0^t \Phi(x, y, z, t)\, dt \quad \text{and} \quad h = \left.\frac{\partial \Psi}{\partial z}\right|_{(x,y,0,t)} \tag{7}$$

The completely hydrodynamic fluid problem requires thus two calculations. The first uses the displacement potential to obtain the real wet surface and the second calculates the hydrodynamic pressure on the wetted surface using the velocity potential. In the displacement potential Ψ case, the limit conditions are similar with those of the velocity potential, Eqs. 1~4, but only the vertical components of Ψ are relevant.

NUMERICAL MODELING

Fluid-heat transfer analogy

The numerical model uses the fluid-head transfer analogy to solve the fluid dynamics problem. Donguy (2002) developed a numerical approach to simulate the slamming problems using this approach under the FE code CASTEM. We have globally followed the same approach using the industrial FE code ABAQUS associated with PYTHON and FORTRAN languages instead of CASTEM. Our developed code was generically named Impact++ ABAQUS after Impact++ CASTEM.

Under the hypotheses of incompressibility and irrotational initial velocity field for the fluid, the temperature T expresses the velocity potential Φ and the displacement potential Ψ. The heat transfer model is given by the following equations:

$$\Delta T = 0 \qquad \text{in the fluid domain } \Omega_f \tag{8}$$

$$\lambda \frac{\partial T}{\partial z} = -\mathbf{q}\cdot\mathbf{z} \qquad \text{on the wetted surface } \Gamma_{FS} \tag{9}$$

$$T = 0 \qquad \text{on the free surface } \Gamma_L \tag{10}$$

$$\frac{\partial T}{\partial z} = \frac{\partial h}{\partial t} \qquad \text{on the free surface } \Gamma_L \tag{11}$$

In Eq. 9, **z** stands for the unit vertical vector. If the temperature T is expressed in [m²/s], the thermal conductivity is set to $\lambda = 1$, and **q** = **-v** = **-grad** Φ is expressed in [m/s] in the head module of ABAQUS/Standard, the above system express the velocity potential problem being similar to system given by Eqs. 1~5. For the displacement potential, we use the same system, Eqs. 8~11, but the temperature T will be consequently expressed in [m²] with thermal conductivity $\lambda = 1$ and $\boldsymbol{q}$ in [m].

Mesh and FE calculations particularities

For a complete analysis of slamming, the total time of analysis is decomposed into major increments of time Δt. The numerical evaluation of the hydrodynamic pressure, Eq. 6, requires at each time increment Δt, two calculations of the velocity potential. A smaller time increment δt is used in order to obtain two velocity potentials at $t_j\,(= j\,\Delta t)$ and $t_j + \delta t$ respectively. In rigid case and only for structures having constant deadrise angles, the value of Δt establishes the frequency of output database. This time increment is also very important for a correct simulation of the fluid-structure coupling in the deformable case. The Δt increment is also an important parameter for a good estimation of $\dot{d}(t)$ by central differencing, Eq. 12. The distances $d(t_i)$ and $d(t_{i-1})$ are the wet surface distances calculated respectively at two consecutives increments t_i and t_{i-1} ($t_i - t_{i-1} = \Delta t$).

$$\dot{d}(t) = \frac{d(t_i) - d(t_{i-1})}{\Delta t} \tag{12}$$

The value of δt depends on the smallest mesh size M_s around the contact surface border and on the wet surface velocity $\dot{d}(t)$. The value of δt must be greater than $M_s/\dot{d}(t)$ to compute accurately the contact surface dimension, but it must be also small enough to determine correctly the pressure field. Finally, a value of $\Delta t/3$ was retained for δt. To obtain accurate values of the wet surface distances at every time increments, we employ numerical iterations with a convergence criterion, Eq. 13:

$$d_k - d_{k-1} \le aprox.\, 2M_s \tag{13}$$

To take into account the high potential gradient, the extremity of the wet surface was meshed with a very fine grid, Fig. 2. In this zone, the smallest mesh size M_s should be lower than the dimension of the physical singularity. The jet thickness δ_{jet} can be a good approximation of this dimension. Nevertheless, the smallest mesh size is determined by the accuracy of $\dot{d}(t)$ which strongly influences the quality of the pressure peak evaluation. We can estimate the logarithmic error of $\dot{d}(t)$ as $\Delta\dot{d}(t)/\dot{d}(t) = M_s/\left(\dot{d}(t)\,\delta t\right)$. In case of wedges and we can prove that the M_s is given by the Eq. 14.

$$M_S = \frac{\pi}{2}\frac{V}{\tan\beta}\delta t\frac{\Delta\dot{d}(t)}{\dot{d}(t)} \text{ where } \dot{d}(t) = \frac{\pi}{2}\frac{V}{\tan\beta} \quad (14)$$

Choosing $\Delta\dot{d}(t)/\dot{d}(t) \le 10^{-2}$, for the least restrictive case (big V and small β) we find $M_s \le 2$ µm, and for the most restrictive case (small V and big β) we find $M_s \le 0{,}4$ µm. We finally chose the smallest mesh size M_s between 1 µm and 2 µm in order to verify the convergence criterion while keeping a reasonable CPU time.

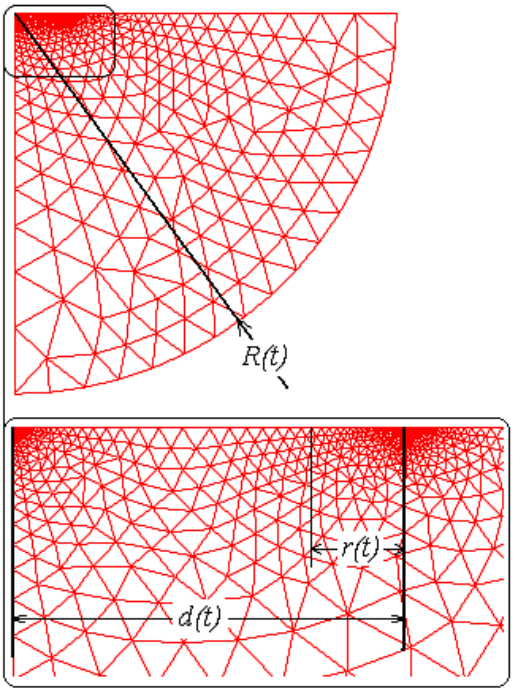

Fig. 2 – Geometric definition

We optimized the fluid mesh reducing the number of elements successively while checking the convergence of the results. The minimal number of elements is approximately between 3000 (at the beginning, first increment) and 5700 (at the end, last increment). The dimension of the meshed fluid zone is dynamically adapted to the contact surface between solid and water $R(t) = 8\,d(t)$, Fig. 2. A smaller value of $R(t)$ implies overestimations of the total effort.

The FE calculations for the displacement potential Ψ employ this type of mesh to compute accurate wet surfaces at each increment of time Δt. The input data in the displacement potential calculus are the positions of the body into the water. The input data in velocity potential Φ calculations are the length of the wet surface and the speed impact of the body into the water. To obtain the velocity potentials we adopted a special technique, valid only for constant entry speed cases and for a given shape form of the rigid body at time. The main idea is to realize a single calculus of the velocity potential Φ and the **grad** Φ considering a reference impact speed of 1 m/s and a reference wet surface of 1 m. This "non-dimensional" calculus will provide the reference velocity potential $\Phi_r(y,z)$ and the reference gradient $\mathbf{grad}\,\Phi_r(y,z)$. These values are fixed for a given shape form of the body. Returning to an Impact++ simulation, after each displacement potential calculus, on the new wet surface $d(t)$, the real potential $\Phi(y, z=0)$ and the real gradient **grad** Φ are obtained using Eq. 15 and Eq. 16 respectively.

$$\Phi(y,0) = V\cdot\Phi_r\left(\frac{y}{d(t)},0\right)\cdot d(t) \quad (15)$$

$$\mathbf{grad}\,\Phi(y,0) = V\cdot\mathbf{grad}\,\Phi_r\left(\frac{y}{d(t)},0\right) \quad (16)$$

where V represents the speed impact of the rigid body. We remark that the velocity potential calculations are independently of deadrise angle β. Using the technique described above, the CPU time is reduced up to 40% compared to the case where the velocity potential Φ was obtained by a FE calculation at each time increment.

Pressure particularities

The calculation of the final pressure is associated with an asymptotic development at the wetted surface boundary. The asymptotic study led to the determination of two zones (inner and far-field) in which two asymptotic developments are obtained. The far-field solution (fulfilling conditions far from the body-surface intersection, but being singular at the intersection, Eq. 17) and the near-field solution (valid near to the intersection, describing the formation of a jet, Eq. 18) have to be connected for the correct evaluation of the resulting total force.

$$p_{far} = -\rho_f\frac{\Phi_{t+\delta t}-\Phi_t}{\delta t} - \rho_f\frac{(\mathbf{grad}\Phi_t)^2}{2} \quad (17)$$

$$p_{near} = \rho_f\frac{\dot{d}(t)^2}{2}\left(1-\left(\frac{1-u}{1+u}\right)^2\right) \quad (18)$$

$$\begin{cases} y-d(t) = \dfrac{\delta_{jet}}{\pi}\left(2\ln u - \dfrac{4}{u} - \dfrac{1}{u^2} + 5\right), & for\ y \le d(t) \\ y-d(t) = \dfrac{\delta_{jet}}{\pi}\left(-2\ln u - 4u - u^2 + 5\right), & for\ d(t) < y \le d(t+\delta t) \end{cases} \quad (19)$$

The variable u is determined by the resolution of the non-linear system given by the Eq. 19. In this equation, the parameter δ_{jet} stands for the jet thickness. Due to divergent flow in axisymmetric configuration, the jet thickness is greater for dihedron case compared to cone case. Eq. 20 gives the jet thickness in 2D. The jet thickness in pseudo-3D case (axi-symmetrical) is provided according to Scolan's investigations (2001).

$$\delta_{jet}^{dihedron} = \frac{\pi}{8}\frac{V^2 d(t)}{\dot{d}(t)^2};\ \delta_{jet}^{cone} = \frac{1}{2\pi}\frac{V^2 d(t)}{\dot{d}(t)^2} \quad (20)$$

Taking into account analytical formula for wet surface $d(t)$ and wet surface velocity $\dot{d}(t)$, a simple calculus shows that the jet thickness is double for dihedron compared to cone, for identical impact speed and deadrise angle, as presented in the Table 1.

Table 1. Analytical formula for dihedron and cone

Case	$d(t)$	$\dot{d}(t)$	δ_{jet}
Dihedron (2D)	$\frac{\pi}{2}\frac{V t}{\tan\beta}$	$\frac{\pi}{2}\frac{V}{\tan\beta}$	$\frac{1}{4}V t\tan\beta$
Cone (pseudo 3D)	$\frac{4}{\pi}\frac{V t}{\tan\beta}$	$\frac{4}{\pi}\frac{V}{\tan\beta}$	$\frac{1}{8}V t\tan\beta$

Since we used numerical resolution and finite distances from the exact wetted surface boundary, an approximate model is necessary to connect analytical far-field and near-field pressure solutions. The operating range of this connection is limited to the distance $r(t) = V\,t$ in front of the end of wet surface, as in Fig. 2, where V is the constant plunging velocity. The connection between far-field and near-field pressures is achieved through the link pressure p_{link}, Eqs. 21~22, and the corrected link pressure ${p_{link}}^c$, Eq. 23:

$$p_{link} = \rho_f \frac{V\,d(t)\dot{d}(t)}{\sqrt{2d(t)(d(t)-y)}} \quad \text{for dihedron} \tag{21}$$

$$p_{link} = \rho_f \frac{V\,d(t)\dot{d}(t)}{\pi\sqrt{d(t)\frac{(d(t)-y)}{2}}} \quad \text{for cone} \tag{22}$$

$$\begin{cases} {p_{link}}^c = p_{link}, \ for\ y \le d(t) - r \\ {p_{link}}^c = p_{far} + \left(\frac{d(t)-y}{r}\right)^2 \left[p_{link} - p_{far}\right], \quad for\ d(t) - r < y \le d(t) \end{cases} \tag{23}$$

To avoid singular values of $\mathbf{grad}\,\Phi(y,z)$ at *(y, z) = (d(t), 0)*, we use $\mathbf{grad}\,\Phi(y,z)$ at *(y_0, z_0) = (d(t) – r, 0)* to evaluate p_{far}, from Eq. 17, in Eq. 23 whatever *y* between *d(t) – r* and *d(t)*. The second order term of this equation must ensure the non-influence of the corrected link pressure into the form of the near-field pressure. The final pressure is given by the sum of the far-field and near-field pressures and subtracting their common part, Eq. 24. The maximal pressure is given by the maximal value of the p_{near}.

$${p_{num}}^f = p_{far} + p_{near} - {p_{link}}^c \ \text{where}\ \dot{d}(t) = \frac{\pi}{2}\frac{V}{\tan\beta} \tag{24}$$

ABAQUS/EXPLICIT APPROACH

Mathematical model of fluid - Fluid Equation of State

The second numerical approach is based on the capabilities of commercial finite element software ABAQUS/Explicit to simulate unsteady fluid flows using Arbitrary Lagrangian-Eulerian (ALE) analysis. This adaptive meshing technique combines the feature of pure Lagrangian analysis and pure Eulerian analysis. According to the ABAQUS documentation (HKS 2004), flow modeling of compressible fluid can be achieved by using the linear U_s-U_p form of the Mie-Gruneisen equation of state. This equation, particularly useful at high pressure, defines the pressure as function of the density ρ and of the internal energy per unit mass E_m of the fluid, Eq. 25.

$$p = f(\rho, E_m) \tag{25}$$

The equation for conservation of energy equates the increase in internal energy per unit mass, E_m to the rate at which work is being done by the stresses and the rate at which heat is being added. In the absence of heat conduction, Eq. 26 gives the energy equation.

$$\rho \dot{E}_m = p\frac{1}{\rho}\dot{\rho} + tr(S\,\dot{e}_d) + \rho\dot{Q} \tag{26}$$

where p is the pressure, S is the deviatoric stress tensor, $\dot{e}_d$ is the deviatoric part of strain rate, and $\dot{Q}$ is the heat rate per unit mass. By eliminating the internal energy from Eq. 25 and Eq. 26, under negligible shear stresses and lack of any heat source assumptions, we obtain the Mie-Gruneisen equation of state, Eq. 27.

$$p - p_H = \Gamma\rho\left(E_m - E_H\right) \ \text{where}\ \Gamma = \Gamma_0\frac{\rho_0}{\rho} \tag{27}$$

where $p_H = f(\rho)$ is the Hugoniot pressure, $E_H = f(\rho)$ is the specific Hugoniot energy, Γ is the Grüneisen ratio given by Equation 30. Γ_0 is a material constant and ρ_0 is the reference density. The linear U_s-U_p Hugoniot form provides the Hugoniot pressure given by the Eq. 28 where η is the nominal volumetric strain $\eta = 1 - \rho_0/\rho$.

$$p_H = \frac{\rho_0 {c_s}^2 \eta}{(1 - s\eta)^2} \tag{28}$$

The terms c_s and s define the linear relationship between the linear shock velocity U_s and the particle velocity U_p, Eq. 29. The term c_s corresponds to the sound velocity at small nominal strains.

$$U_s = c_s + sU_p \tag{29}$$

With the above assumptions, the Eq. 30 gives the pressure in the fluid.

$$p = \frac{\rho_0 {c_s}^2 \eta}{(1 - s\eta)^2}\left(1 - \frac{\Gamma_0\eta}{2}\right) + \Gamma_0\rho_0 E_m \tag{30}$$

The classical Newtonian fluid model defines the deviatoric response of the fluid, Eq. 31. In below equation, σ_D is the deviatoric stress, $\hat{D}_D$ is the deviatoric rate-of-deformation tensor and μ is the viscosity of the fluid respectively.

$$\sigma_D = 2\mu\,\hat{D}_D \tag{31}$$

The equation of state can be used with all solid continuous elements (excepting elements working in plan strain case). Thus, we model the fluid with solid elements that have properties of fluid. In our simulations, the equation of state is defined by the parameters presented in Table 2.

Table 2. Equation of state parameters – ABAQUS/Explicit ALE

c_0 [m.s^{-1}]	s [-]	Γ_0 [-]	μ [-]	[kg.m^{-3}]
1425	1.75	0.28	0.001	1000

FE modeling

As in Impact++ ABAQUS simulations, the fluid domain must be greater then the solid dimensions in order to avoid the numerical errors and not overestimate fluid pressures. In the present approach, the fluid is compressible. Waves in compressible media travel at finite speed. Therefore, the pressure acting on the structure will not depend on the size of the fluid domain if the non-return of shock waves condition,

Eq. 32, is satisfied. In this relation, L is the minimal distance between the structure and the limits of the fluid domain at maximum draught and T is the time of the simulation.

$$L \geq c_0 T/2 \tag{32}$$

To minimize the CPU time, only in the superior part of the fluid, near to the structure, the mesh uses 4-node quadrilateral elements with bilinear interpolation functions and reduced integration (CPE4R in the plane strain problems and CAX4R for axisymmetric problems). In order to prevent severe mesh distortion, the very fine fluid mesh (element size about 150 µm) is associated with the adaptive meshing technique. The inferior part of the fluid, in which the deformation of the fluid remains moderate, is modeled with a Lagrangian mesh using triangular linear elements (CPE3 or CAX3). The Fig. 3 shows the fluid mesh near to the structure.
Having one integration point only, the CPE4R and CAX4R elements may suffer from hourglassing. It is possible for them to distort in such a way that the strains calculated at the integration point are zero, which, in turn, leads to uncontrolled distortion of the mesh. In order to prevent this phenomenon, the elements include an hourglass control type "Combined" which associates a stiffness and viscous term, Eq. 33.

$$Q = \frac{1}{2}\left(K\, q + C\, \frac{dq}{dt} \right) \tag{33}$$

The term q is an hourglass mode, Q is the force (or moment) conjugated to q, and K and Q are stiffness and viscous coefficients. The stiffness term acts to maintain a nominal resistance to hourglassing throughout the simulation, whereas the viscous term generates additional resistance to hourglassing under dynamic loading conditions.

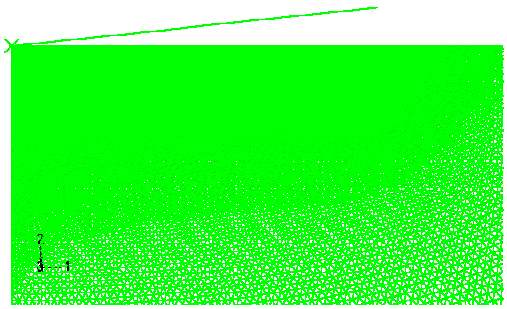

Fig. 3 – Fluid mesh near to the structure - ABAQUS/Explicit

To model the interaction between the structure and the fluid, we adopt a frictionless contact type. In the ABAQUS software, several methods are available for modeling the contact interface behavior. By default, a "hard" contact pressure-overclosure relationship is proposed for both surface-based contact and element-based contact. This type of contact do not allows penetration between surface (impenetrability condition) and conducts in our case to high oscillations of the peak pressure. In our simulations, we have used the "softened" pressure-overclossure relationship, which leads to a regularization of the impenetrability condition. The pressure-overclosure relation is prescribed by using an exponential law, presented in Fig. 4.

This law depends on two principal parameters: c_0 and p_0. The surfaces begin to transmit contact pressure once the clearance between them, measured in the contact (normal) direction, reduces to c_0. The contact pressure transmitted between the surfaces then increases exponentially as the clearance continues to diminish.

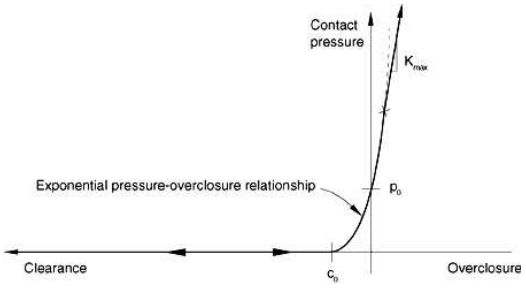

Fig. 4 – Exponential "softened" contact

These two parameters should be carefully selected such that inter-penetrations between the fluid and solid surfaces remain small. Constantinescu (2006) performed a parametric study to understand the effect of these parameters. He observed that it is possible to obtain smooth solutions using very small interpenetrations between the surfaces (of the order of 10 µm). By combining these parameters with those presented in Table 2, we obtain good results concerning the movement of fluid, Fig. 5, but also for spatial and temporal pressure, and effort distribution in rigid case for wedges and cones comparing with results issued from Impact++ ABAQUS and FLUENT codes. The results are presented later in this paper.

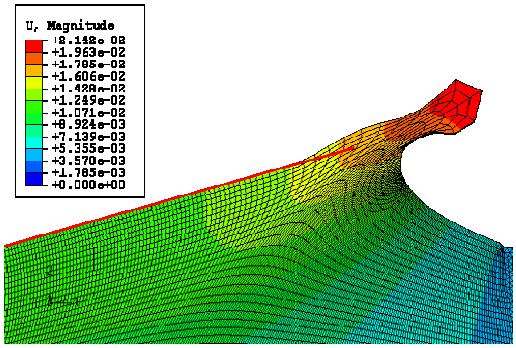

Fig. 5 – Structure entirely immersed

This approach has some advantages over the Impact++ approach. Thus, the modeling is not restricted to moderate deadrise angles. More important, it allows to deals with 3D problems. The slamming phenomena in deformable case can be directly treat within Abaqus, without rely on the coupling of other software product for the structure.

COUPLED EULERIAN - LAGRANGIAN (CEL) APPROACH

The pure Eulerian analysis capability in Abaqus/Explicit allows for effective modeling of applications involving extreme deformation, including fluid flow. The Eulerian capability can be coupled with traditional Lagrangian capabilities to model interactions between highly deformable materials and relatively stiff bodies, such as in fluid-structure interactions. The principle of calculation is based on the Volume of Fluid method (VOF). The method is based on a fraction function, commonly denoted C.

It is defined as the integral of fluid's characteristic function in the control volume , namely volume of a computational grid cell. Thus, inside each cell of the eulerian mesh, the scalar variable C increases gradually as the fluid moves into the cell. Basically, when the cell is empty (there's no traced fluid inside) value of C is zero, if cell is full, we have $C = 1$.

This recent possibility offered by ABAQUS remains for the moment limited to 3D models and eulerian field meshed using brick elements. For this reason we could not benefit completely from the axi-symmetry of the problem of which we modeled the quarter, as showed in Fig. 6. The quarter of cone is represented by a non-deformable rigid body. The volume of water is represented by a cube having an edge length of 0.8 m. The superior zone of the mesh (thickness of 0.05 m) is represented by vacuum zone. The fluid and vacuum zones constitutes the eulerian domain. The mesh grid remains very perfectible, but it allows obtaining suitable hydrodynamic efforts using approximately 410000 elements. According to Fig. 6, the finest grid is localized near to the interaction zone between the cone and water. Inside this cubic zone (edge length 0.2 m), the dimension of the mesh elements is around 5 mm.

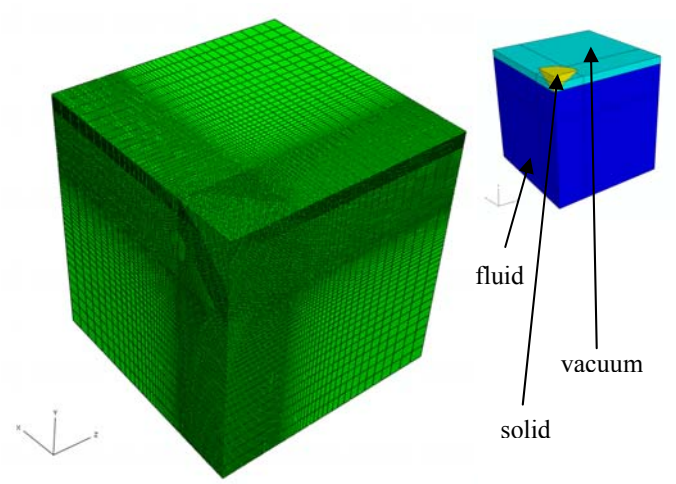

Fig. 6 – Fluid, vacuum and cone domains and meshes

ABAQUS/Explicit CEL method uses the same equation of state as ABAQUS/Explicit ALE, equation already presented in the previous section. Only its parameters are slightly different, Table 3.

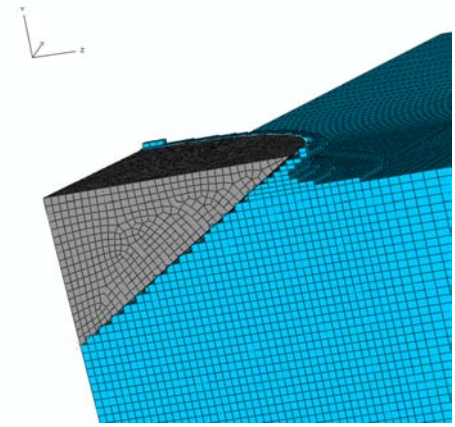

Fig. 7 – Fluid deformation 3.6 ms after impact, cone, deadrise angle 30°, impact velocity 20 m/s

Table 3. Equation of state parameters – ABAQUS/Explicit CEL

c_0 [m.s^{-1}]	s [-]	Γ_0 [-]	μ [-]	[kg.m^{-3}]
1414	0	0	0.001	1000

The contact between the cone and water is modeled using frictionless hard contact model. Excepting the two inside surfaces of the fluid domain and the free face of the empty field, the three exterior faces of the eularian field are regarded as “stick” walls where the three components material speeds are null. The quality of the grid mesh does not allow to represent accurately the formation of the jet. However, we observe the formation of waves and we correctly verify the axisymmetry of the problem, according to the Fig. 7.

EXPERIMENTAL INVESTIGATIONS

Experimental set-up

At ENSIETA laboratory, we carried out experimental tests in order to obtain experimental data to validate the previous numerical approaches. The investigation consists of impact tests with simple structures using a hydraulic shock machine, presented in Fig. 8. This machine is rather unique according to its performances and its flexibility for the reason that crushing test on solids can be also conducted. Its numerical control with internal model allows controlling the displacement and the impact velocity of the plunger piston.

The structure is fixed at the extremity of the plunger piston through an intermediate support, as presented in Fig. 10. The fluid tank is mounted under the shock device and is filled with 1.1 m height of fresh water.

Fig. 8 – **Shock machine and its water tank**

We have tested three types of cones (7°, 15° and 30° deadrise angles). The design of these three structures must respect certain conditions. The structure is made in massive aluminum alloy to assure minor inertial forces and very small overall deformation. For cones, the deadrise angle β must allow an easier visualization of the free water surface. The impact force should be high enough in order to guarantee a satisfactory signal/noise ratio, but must not overstep the shock machine limits. For each type of structure, several Impact++ ABAQUS simulations allowed to calculate the maximal force and thus to estimate the optimal impact velocity.

The flow experiment in semi-infinite medium is ensured by the ratio between dimensions of the tank and those of the structures. In order to avoid boundary effects, the maximum diameter of these parts must be lower than 1/6th of the smaller characteristic length of the basin (i.e. the

width). After diameter and deadrise angle settlement, the height of parts was determined with respect to a stiffness criterion. This criterion corresponds to a deflection of the structure's end (noted **A** on Fig. 9) smaller than 50 μm, which corresponds to the manufacture tolerance. The geometries were numerically tested with ABAQUS/Standard in order to obtain this maximal deflection. The Fig. 9 presents the final dimensions of the aluminum alloy cone having a β = 7° deadrise angle.

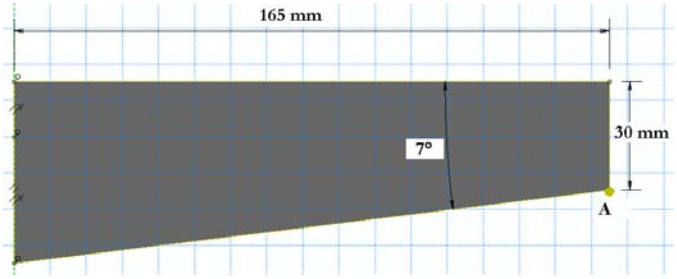

Fig. 9 – Positioning of the point A which corresponds to maximum displacement under flexion (case of cone β = 7°)

The use of the Eq. 35 combined with the Wagner's linearized theory made it possible to identify the "ideal" points of functioning for the tests relatively to machine capability, namely:

- V_{max} = 10 m/s for β = 7° with a maximal force F ≈ 91.4 kN;
- V_{max} = 16 m/s for β = 15° with a maximal force F ≈ 98.0 kN;
- V_{max} = 20 m/s for β = 30° with a maximal force F ≈ 42.8 kN.

Table 4 presents the various impact velocities employed for each type of cone. In order to ensure the results reproducibility, each test has been repeated at least three times.

Table 4. Set of deadrise angles and impact velocities used in experiments

Deadrise angle β	7°	15°	30°
Impact velocities [m/s]	5.0; 6.5; 8.0	8.0; 12; 15.0	15.0; 18.0; 20.0

Experimental instrumentation

During the impact tests, displacement, acceleration and force measurements are performed. An internal machine sensor measures the piston displacement at 2.5 kHz sampling frequency. A piezoresistive sensor type EGAS-FS-*-250-/V12/L8M/X, placed on the cone, measures the acceleration, Fig. 10. It has an effective range of ± 250 g, a sensitivity of 0.32 mV/g, an eigen-frequency of 2.5 kHz, a damping coefficient of 0,64 and a voltage supply of 12 V. The acceleration measurements allow us to quantify the inertial forces due to slightly non-constant velocity during the impact.

Four FFG-2-1K-C1-11 KYOWA™ gauges located at 50 mm from the piston extremity measure the impact force, Fig. 10. The KYOWA gauges are connected in Wheatstone full bridge to a NICOLET™ data acquisition system recording at a sampling rate of 20 kHz. The electrical signal delivered by the acceleration sensor is recorded on the same data acquisition system at the same sampling frequency. We have also used an electrical detection system to identify correctly the real time contact between the cone and water. In fact, this time represents the start of the numerical simulations. The NICOLET™ data acquisition system records the voltage in an electrical circuit that changes its impedance when the cone touches the water.

The force gauges were already calibrated in order to establish a relation between the force F and the variation of relative voltage variation Δu/U at the terminals of the Wheatstone bridge. The speed and the displacement are calculated successively by a simple and double numerical integration of the acceleration signal. An optimization procedure of the displacement and a temporal retiming made it possible to calibrate the accelerometer and to obtain the inertial efforts. The results show, on one hand, that the stabilized impact speed is not strictly constant and, on the second hand, that resultant accelerations are more disadvantageous as the mass of the structure is important.

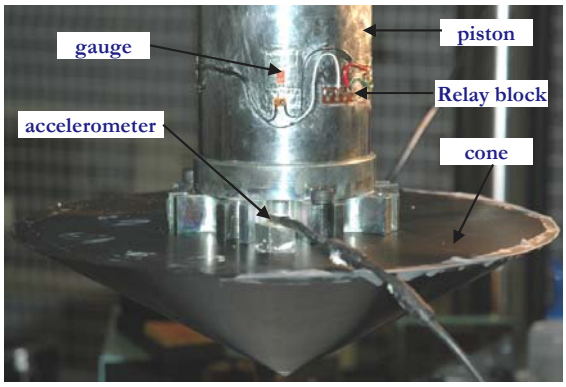

Fig. 10 – Accelerometer implantation and gauges positioning

In addition to basic acquisition systems (force, displacement, acceleration), we also used a PHOTRON high speed digital video camera to record the evolution of the interaction between cone and water in a window of 1024x128 pixels at 15000 frames per second. For this purpose, the camera is placed near to a circular window of the lateral side of the basin, Fig. 8. These circular windows, having a diameter of 0.7 m, are made in PMMA (PolyMethyl MethAcrylate). The Fig. 11 shows several photos of this fluid-structure interaction during the impact of the 15° deadrise cone.

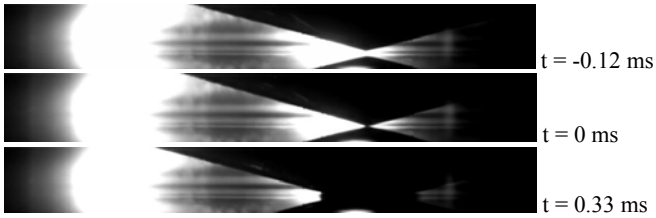

Fig. 11 – Photos of the impact of a 15° deadrise angle cone at 15 m/s

COMPARISON OF RESULTS

Comparisons between numerical approaches

Initially, we compared the results obtained using Impact++ ABAQUS with those of Impact++ CASTEM. The main differences between the two codes refer to calculus of the wet surface extend *d(t)* and to calculus of the inner pressure for cones. Donguy (2002) used an analytical estimation of *d(t)*, whereas we employ an iterative process with convergence criterion. In case of cones, Donguy do not correct the inner pressure and the analytical correction formula for cones, and applied the equations used for the wedge case. However, in our simulations the maximum pressure values agree very well with those determined with CASTEM (Constantinescu 2006). We also obtain the same wet surface propagation velocity, as well as the resulting vertical force on the solid.

The first comparisons between Impact++ ABAQUS and ABAQUS/Explicit reveal satisfactory results concerning spatial and temporal pressures, and effort distribution. As shown in Fig. 12, with ABAQUS/Explicit the pressure peaks evolution of spatial distributions is well reproduced regarding the Impact++ results. Initially, the ABAQUS/Explicit response has an oscillatory due to initial contact between solid and fluid that repose on a small number of elements mesh, and then it stabilizes.

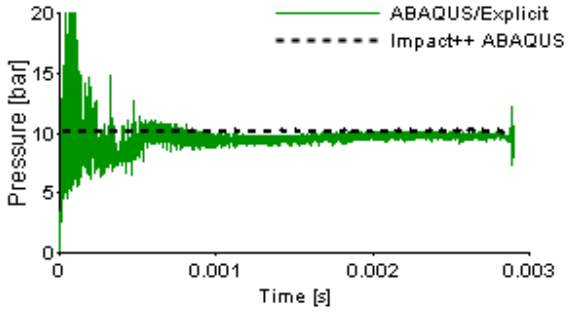

Fig. 12 – Peaks pressure evolution for a rigid wedge β = 10°, V = 5 m/s

We also observed a good agreement between the Impact++ and the theoretical model of Zhao and Faltinsen (1993), with a maximal discrepancy of results around 10%. This difference is explained by geometric non-linearity of the Zhao and Faltinsen model in opposition to the Impact++ ABAQUS linearization. ABAQUS/Explicit and FLUENT calculations confirmed this fact. As we can see in Fig. 13, the five models forecast also very near values regarding the wet surface propagation velocity and maximal peak pressure. The pressure time histories are calculated at point P, disposed on the structure generatrix at 90 mm from the top of the wedge. The results obtained with ABAQUS/Explicit are very close to those of fully CFD software FLUENT.

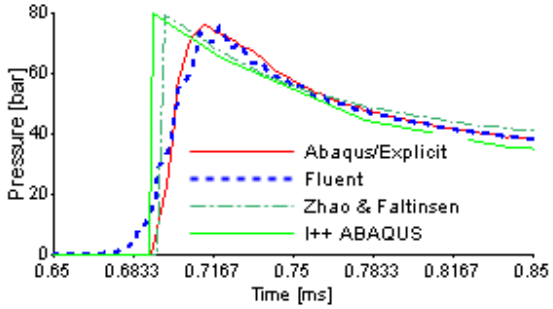

Fig. 13 – Pressure vs. time at points P for a wedge, deadrise angle 14°, impact velocity 20 m/s

The main result for rigid wedges is the evolution of the dimensionless expression $f(\beta)$ expressed by the Eq. 34, associated to the force per unit length F which is function of time t, deadrise angle β, fluid density ρ_f and entry speed V.

$$f(\beta) = \frac{F \tan^2 \beta}{\rho_f V^3 t} \qquad (34)$$

According to the Fig. 14, the hydrodynamic forces predicted by models based on Wagner's theory, i.e. Impact++ (for small deadrise angles β) and Zhao and Faltinsen analytical model, are higher compared to "non-linear" models, i.e. ABAQUS/Explicit, Fluent and Zhao and Faltinsen numerical model.

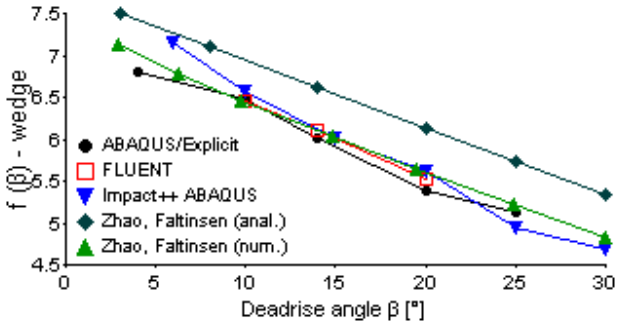

Fig. 14 – Evolution of non-dimensionalized force function of deadrise angle for rigid wedges

Regarding the cone case, we establish similar results to the wedges case concerning the total force. Thus, the hydrodynamic force predicted by Impact++ is slightly superior compared to Fluent and ABAQUS/Explicit results, Fig. 15. There again, the discrepancy is also around 10%. On the other hand, ABAQUS/Explicit results remain in very good agreement with those of FLUENT.

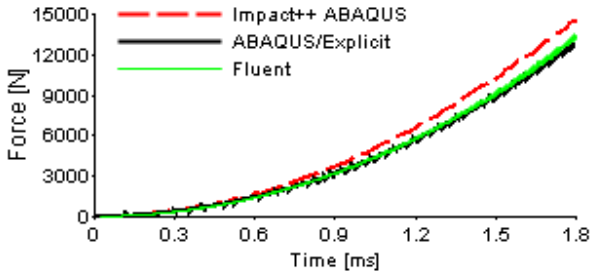

Fig. 15 – Force vs. time for cone of 6° deadrise angle and impact velocity of 5 m/s

Concerning the third approach, ABAQUS/Explicit CEL provides very good results compared to Impact++ ABAQUS. In Fig. 16, the temporal evolutions of the effort obtained with the two codes are almost overcome.

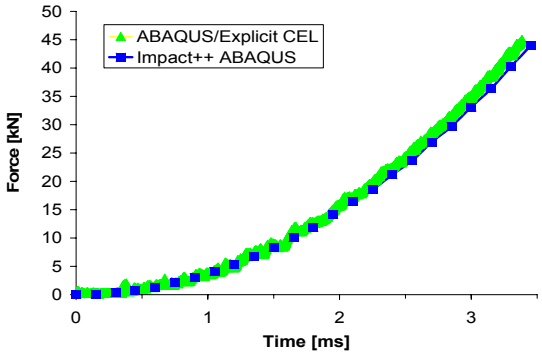

Fig. 16 – Force vs. time for a cone, deadrise angle 30°, V = 20 m/s

Comparisons between numerical and experimental results

We present in this section the experimental results obtained for the three rigid cone models having deadrise angle β = 7° or 15° or 30°. The impact speed is controlled with a small error (less than 5%) which enables us to suppose that it is constant during the penetration of the

structure. During the penetration of the cone into the water, the force increases up to a maximum value then, it falls brutally. This last phenomenon (loss of force) corresponds to the situation where the cone is entirely immersed and was also demonstrated numerically by Impact++ ABAQUS and ABAQUS/Explicit simulations. Moreover, according to the dimensional theory, the time evolution of the hydrodynamic force is parabolic for a rigid cone. That corresponds well to the experimental results, as presented in Fig. 17.

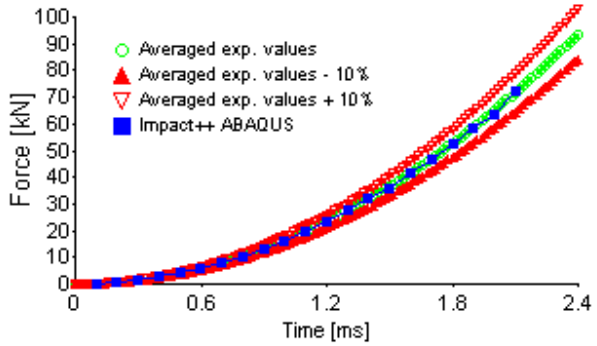

Fig. 17 – Force vs. time for a cone, deadrise angle 15°, V = 15 m/s

In Fig. 17, beside the Impact++ ABAQUS results, we have represented the experimental average values obtained for the effort, as well as their upper and lower experimental limits. A statistical study reveals a high probability (90%) to obtain these experimental results.

In this context, the 7° deadrise angle case is less restrictive for the iterative calculus of *d(t)* and induce numerical errors. Thus, the numerical results are slightly higher than the experimental values. The 15° and 30° deadrise angle cases are most restrictive and this fact implies a very good agreement between the numerical and averaged experimental results, Fig. 16.

We have also chosen to compare the experimental results to those obtained numerically using the "non-dimensionalized" parameter related to the force. Equation 35 gives the expression of this dimensionless parameter of slamming for cones.

$$f(\beta)=\frac{F\tan^3\beta}{\rho_f V^4 t^2} \qquad (35)$$

In the first instants of plunging, $f(\beta)$ is badly calculated since the measured effort F and the time t are almost zero (zero force divided by zero time). Afterwards, $f(\beta)$ tends to an "asymptotic" value until the end of test (maximal impact force), as for wedge case. The simulations and the experiments confirmed well this assertion. The error made to calculate $f(\beta)$, Eq. 35, is evaluated thanks to Eq. 36.

$$err\_f(\beta)=\frac{|\Delta F|}{F}+4\frac{|\Delta V|}{V}+2\frac{|\Delta t|}{t} \qquad (36)$$

In order to determine with precision the "asymptotic" value of $f(\beta)$, we chose to preserve the points such as $err\_f(\beta) \leq 10\%$ then we made the average of the values of $f(\beta)$ which check this condition. The Table 5 presents the average values of $f(\beta)$ obtained experimentally and using different FE codes, for different deadrise angles β.

Table 5. Averages values of $f(\beta)$

Deadrise angle	7°	15°	30°
Number of tests	11	9	10
Tolerated error for experiments	10 %		
$f(\beta)$ experimental	6.79	6.18	4.75
$f(\beta)$ Impact ++ ABAQUS	7.27	6.11	4.44
$f(\beta)$ ABAQUS/Explicit	7.18	6.25	4.65
$f(\beta)$ FLUENT	7.20	6.26	4.68

For each entry speed, the tests generate force signals and values of $f(\beta)$ appreciably equivalent, hence the phenomenon can be considered reproducible. The numerical and experimental studies show the non-dimensional parameter of slamming is mainly controlled by the deadrise angle of the cone. Its value is constant in time and the mass or entry speed does not influence it. The Table 5 shows a good results agreement between experiments, Impact++ ABAQUS, ABAQUS/Explicit and FLUENT.

Fig. 18 shows the evolution of $f(\beta)$ according to time. The time t = 0 corresponds to the top of contact between cone and water, detected by the electrical system. Impact++ ABAQUS and experimental results for $f(\beta)$ are found to be in good agreement.

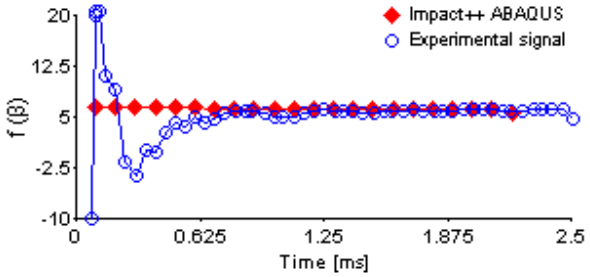

Fig. 18 – Impact++ ABAQUS and experimental non-dimensionalized forces (cone, β = 15°)

In order to a have a global comparison between experimental and numerical results for cones, we represent in the Fig. 19 the evolution of the non-dimensionalized expression $f(\beta)$ expressed by the Eq. 35, for different deadrise angles β. The experimentally hydrodynamic forces are very close to those obtained numerically. When the steady state dynamic pressure term is neglected in Eq. 6 (or Eq. 17), Impact++ ABAQUS supplies a 'linear' solution higher compared to the "non-linear" solution.

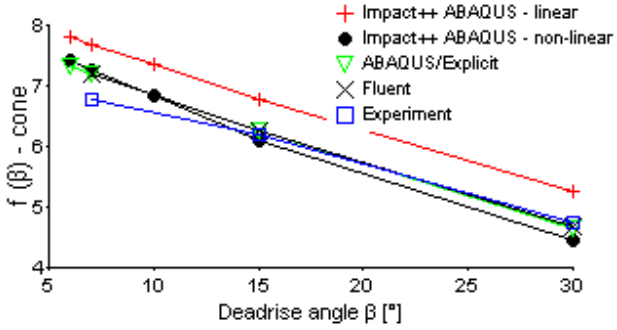

Fig. 19 – Evolution of non-dimensionalized force function of deadrise angle for rigid cones

CONCLUSIONS

We presented in this paper three numerical approaches able to solve two-dimensional slamming problems. An experimental work completes the research work and allows to validate the numerical tools. We have described the experimental process, including the equipment presentation, the measurement instruments and methods, as well as the choice and the dimensioning of the impacted structures. We tested two types of structure, a cone and a segment of sphere, but the results refer only to the rigid cones impacting a free water surface. The numerical and experimental efforts are in good agreement. Taking into account the asymptotic values of the non-dimensionalized parameter of slamming $f(\beta)$, well-predicted by the experimental results, we appreciate that the numerical results were well confirmed by these first experimental tests.

Concerning the numerical models, we described firstly the Impact++ ABAQUS approach for which the fluid problem is described by a potential formulation and an asymptotic method. The hydrodynamic pressure is corrected by analytical formula in order to take into account the formation of the jet. The pressure formulae are different between cone and wedge cases. These hybrid fluid-thermal approaches using CASTEM or ABAQUS FE codes give similar results for the propagation velocities of wetted surface and approximately 5% discrepancy for maximal pressure. The CPU time was considerably reduced using a special technique that allows to calculate velocity potentials at each time increment from an non-dimensional solution. We mention that each structure (each shape form) has its own solution. This technique must be used only for rigid structures.

ABAQUS/Explicit ALE (Arbitrary Lagrangian-Eulerian) represents the second numerical approach. It was developed initially to validate the Impact++ results, but we perceive quickly its potential in deformable and fully 3D cases. This code does not allow determining accurate pressure peaks values without very fine mesh and implicitly high CPU cost, but reliable accurate information is obtained for the resulting effort. Nevertheless, the results still rather dependent on coefficients of exponential "softened" contact law. A special attention must be accorded to this step in order to obtain a broadly contact model. Excessive grid mesh distortions were also observed during the final phase of the simulation. Globally, the ABAQUS/Explicit results are in good agreement with Impact++ ABAQUS results and particularly with those of FLUENT.

Finally, ABAQUS/Explicit CEL (Coupled Eulerian-Lagrangian) approach seems to provide very interesting and good results compared to other numerical and experimental results, right after our first simulations. This approach proves to be a potential way to study 3D slamming notwithstanding certain limitations.

ACKNOWLEDGEMENTS

We are grateful to Steven Kerampran from ENSIETA, Brest, for supplying numerical results with the CDF code FLUENT, to University of Liege for the Post-doctoral Fellowship and the MARSTRUCT FP6-PLT-506141 EU Project. We are also thankful to DGA/MRIS for financial support in the experimental study of slamming.

REFERENCES

Bertram, V. (2002). "*Practical Ship Hydrodynamics*", Butter-worth + Heinemann Oxford

Constantinescu, A. (2006). "*2D modeling of the impact of a body on water. Damage initialization*", Ph.D. Thesis, ENSIETA, Brest, France

Donguy, B. (2002). "*Study of the fluid interaction structure at the time of the hydrodynamic impact*", Ph. D. Thesis, ECN, Nantes, France

Hibbit, Karlsson, and Sorensen Inc. (2004). "*ABAQUS Analysis User's Manual. Volume V: Prescribed Conditions, Constraints & Interactions*"

Karman, T. von (1929). "*The impact of seaplane floats during landing*", NACA Technical Notes 321

Langrand, B., and E. Deletombe (2001) "*De la validité des comparaisons calculs/essais dans les problèmes couplés fluide/structure*", 15th French Congress of Mechanics, Nancy, France

Scolan, Y.M., and A. A. Korobkin (2001). "*Three-dimensional theory of water impact. Part 1. Inverse Wagner problem*", Journal of Fluid and Mechanics, Vol. 440, pp. 293-326

Zhao, R., and O. M. FaltinseN (1993). "*Water entry of two-dimensional bodies*", Journal of Fluid Mechanics, Vol. 246, pp. 593-612

Wagner, H. (1932). "*Über Stoss-und Gleitvorgänge an der Oberfläche von Flüssigkeiten*", ZAMM, Vol. 12, pp. 193-215